Age-dependent dose calculations for common PET radionuclides and brain radiotracers in nonhuman primate computational models

Tianwu Xie [a)]
Institute of Radiation Medicine, Fudan University, 2094 Xietu Road, Shanghai 200032, China
Division of Nuclear Medicine and Molecular Imaging, Geneva University Hospital, Geneva CH-1211, Switzerland

Xin Chen
Institute of Radiation Medicine, Fudan University, 2094 Xietu Road, Shanghai 200032, China

Habib Zaidi
Division of Nuclear Medicine and Molecular Imaging, Geneva University Hospital, Geneva CH-1211, Switzerland
Geneva Neuroscience Center, Geneva University, Geneva CH-1205, Switzerland
Department of Nuclear Medicine and Molecular Imaging, University of GroningenUniversity Medical Center Groningen, Groningen, Netherlands
Department of Nuclear Medicine, University of Southern Denmark, Odense DK-500, Denmark

(Received 2 April 2020; revised 20 May 2020; accepted for publication 4 June 2020; published 13 July 2020)

Purpose: The combination of nonhuman primates (NHPs) with the state-of-the-art molecular imaging technologies allows for within-subject longitudinal research aiming at gaining new insights into human normal and disease conditions and provides an ideal foundation for future translational studies of new diagnostic tools, medical interventions, and therapies. However, radiation dose estimations for nonhuman primates from molecular imaging probes are lacking and are difficult to perform experimentally. The aim of this work is to construct age-dependent NHP computational model series to estimate the absorbed dose to NHP specimens in common molecular imaging procedures.
Materials and methods: A series of NHP models from baby to adult were constructed based on nonuniform rational B-spline surface (NURBS) representations. Particle transport was simulated using Monte Carlo calculations to estimate S-values from nine positron-emitting radionuclides and absorbed doses from PET radiotracers.
Results: Realistic age-dependent NHP computational model series were developed. For most source-target pairs in computational NHP models, differences between C-11 S-values were between −13.4% and −8.8%/kg difference in body weight while differences between F-18 S-values were between −12.9% and −8.0%/kg difference in body weight. The absorbed doses of ^{11}C-labeled brain receptor substances, ^{18}F-labeled brain receptor substances, and ^{18}F-FDG in the brain ranged within 0.047–0.32 mGy/MBq, 0.25–1.63 mGy/MBq, and 0.32–2.12 mGy/MBq, respectively.
Conclusion: The absorbed doses to organs are significantly higher in the baby NHP model than in the adult model. These results can be used in translational longitudinal studies to estimate the cumulated absorbed organ doses in NHPs at various ages. © *2020 American Association of Physicists in Medicine* [https://doi.org/10.1002/mp.14333]

Key words: computational models, Monte Carlo simulations, molecular imaging, nonhuman primates, radiation dosimetry

1. INTRODUCTION

The nonhuman primate (NHP) is the gold standard animal model for evaluating the response of the human body to radiation exposure owing to similarities between its organ structures, genome, life span, and metabolism. The validation of novel imaging biomarkers in NHP models is important in both animal-based preclinical studies and translational research in humans. The NHP has close homology to humans in terms of metabolism, developmental or aging processes, and molecular target distributions.[1] For example, NHPs and humans share more than 95% of overall gene homology while the reported differences in neuron innervation between monkey and rodent may be indicative of the differences in the biodistribution, pharmacokinetic and pharmacodynamic interactions of drugs and tracers within the neuronal system.[2,3] Using animal models with receptor localization and target distribution resembling those of humans is critical for generalizing outcomes of preclinical studies to human conditions in PET-based molecular imaging research.[4] Prior knowledge of the biodistribution of PET tracers in NHPs can be exploited to estimate the absorbed dose in humans, to provide information about the occupancy of receptor systems and to gain a better understanding of the tracer kinetic properties.[5,6] An additional advantage of NHPs in preclinical research is their potential use in longitudinal studies in laboratory settings where baseline physiological and biochemical measurements can be correlated with changes on researched

subjects while experimental manipulation is performed over many years. Another potential application of NHPs is the *in vivo* measurement of blood flow or energy use by the central nervous system using PET imaging where ^{15}O-H_2O and ^{18}F-FDG are commonly used to characterize the neural activity.[7,8] To the best of the authors' knowledge, the radiation dose to NHP in preclinical PET studies has been reported only in few studies.[9,10] It was recently observed that low dose (50 mGy–1 Gy) of ionizing radiation can stimulate the secretion of cytokines and promote the innate immune response in mammal subjects.[11] Therefore, estimation of absorbed doses from radiotracers in NHPs in longitudinal studies is highly desired, especially for studies involving PET imaging of protein aggregation and neurodegenerative diseases. In this regard, the development of realistic computational models mimicking the anatomy of NHPs is of paramount importance.[12]

In this work, we used the original nonuniform rational B-spline surface (NURBS)-based NHP model developed by our group[13] to produce a series of models representing NHPs at 5 age periods (baby, infant, juvenile, young, and adult) between newborn and 192 months. Similar work was reported previously for computational rat models.[14] Monte Carlo-based particle transport simulations of energy spectra corresponding to decay schemes of positron-emitting radionuclides (C-11, N-13, O-15, F-18, Cu-64, Ga-68, Rb-82, Y-86, and I-124) were performed to calculate the absorbed fractions and S-values for the considered series of NHP models. The obtained radiation dosimetry database was used to assess the radiation dose from ^{11}C-labeled brain receptor substances, ^{11}C-labeled substances (realistic maximum), ^{15}O-H_2O, ^{18}F-labeled brain receptor substances, and ^{18}F-FDG in NHPs at different age periods. The realistic maximum model assumes that half of the decays occur while the substance passes the bladder, while the remaining disintegrations occur homogeneously in the body. The radiation doses to NHP subjects in longitudinal studies were estimated and discussed.

2. MATERIALS AND METHODS

2.A. Construction of computational NHP models

Given that the rhesus monkey is one of the most popular NHP strains used in preclinical research, we developed a series of anatomic models based on the original NURBS-based realistic NHP model[13] derived from digital cryosection images of an 8-year-old female rhesus monkey according to published morphologic parameters and the body growth curve for this NHP species. The age, weight, and crown-rump length values summarized in Table I were obtained from 5-yr study data on the clinically healthy rhesus macaques[15] and used as basis for modification of the original NURBS-based NHP model (anchor model). The models representing baby, infant, juvenile, young, and adult NHP subjects were constructed by scaling the anchor model to fit the target morphologic parameters using the Rhinoceros™ package. The deformation process includes three main steps. In the first step, the crown-rump length of the anchor model is measured and a scaling factor calculated as the ratio of aim crown-rump length and the original crown-rump length:

$$F_z = \frac{\text{Length}^{Aim}_{\text{Crown-rump}}}{\text{Length}^{Anchor\,model}_{\text{Crown-rump}}} \quad (1)$$

where the scaling factor F_z is used as input parameter for 1D scale of the anchor model at crown-rump direction in Rhinoceros™. Once the crown-rump length has been adjusted to achieve the target values, in the second step, the body weight of the modified model is determined as the sum of organ masses. Subsequently, the model is modified to match the targeted body weight. The aimed body weight is achieved by scaling the previous model in the two dimensions of the sagittal plane, which involves iterating between estimating the total body weight and adjusting the scaling factors for body contour and internal organs. The organ mass is calculated as the product of the organ volumes and their corresponding densities obtained from the ICRP report 89[16] while the body weight is calculated as the sum of masses of identified organs. The final step consists in voxelizing the remodeled NHP model into a voxel model using the Binvox package.[17,18]

Figure 1 shows 3D visualizations of the developed NHP model series. The skeleton system was updated by identifying the mineral bone, red bone marrow (RBM), and yellow bone marrow (YBM) from the original color skeleton slice images using thresholding-based segmentation.[19] Figure 2 shows the skeletal system of the developed NHP models, including mineral bone, RBM, and YBM.

2.B. Monte Carlo simulations

The computational NHP models were used as input to the MCNPX Monte Carlo code[20] for simulation of the transport and interaction of the emitted radiation. A uniform voxel dimension of $2 \times 2 \times 2$ mm^3 was set for all NHP models to minimize the simulation differences. The chemical composition of each organ and tissue is assumed to be the same as humans and was obtained from the ICRP report 89 (ICRP 2002). Uniformly distributed C-11, N-13, O-15, F-18, Cu-64, Ga-68, Rb-82, Y-86, and I-124 sources were simulated in 33 identified organs for the five constructed NHP models. The decay schemes of the considered radionuclides were obtained from the Health Physics Society.[21] The absorbed fractions

TABLE I. Morphometric data of rhesus monkeys.[15]

Models	Age (Month)	Weight (kg)	Crown-rump length (cm)
Baby	0–6	1.1	23.07
Infants	7–18	2.55	30.96
Juveniles	19–31	3.49	35
Young	32–44	5.22	39
Adult	45–192	8.58	44.28

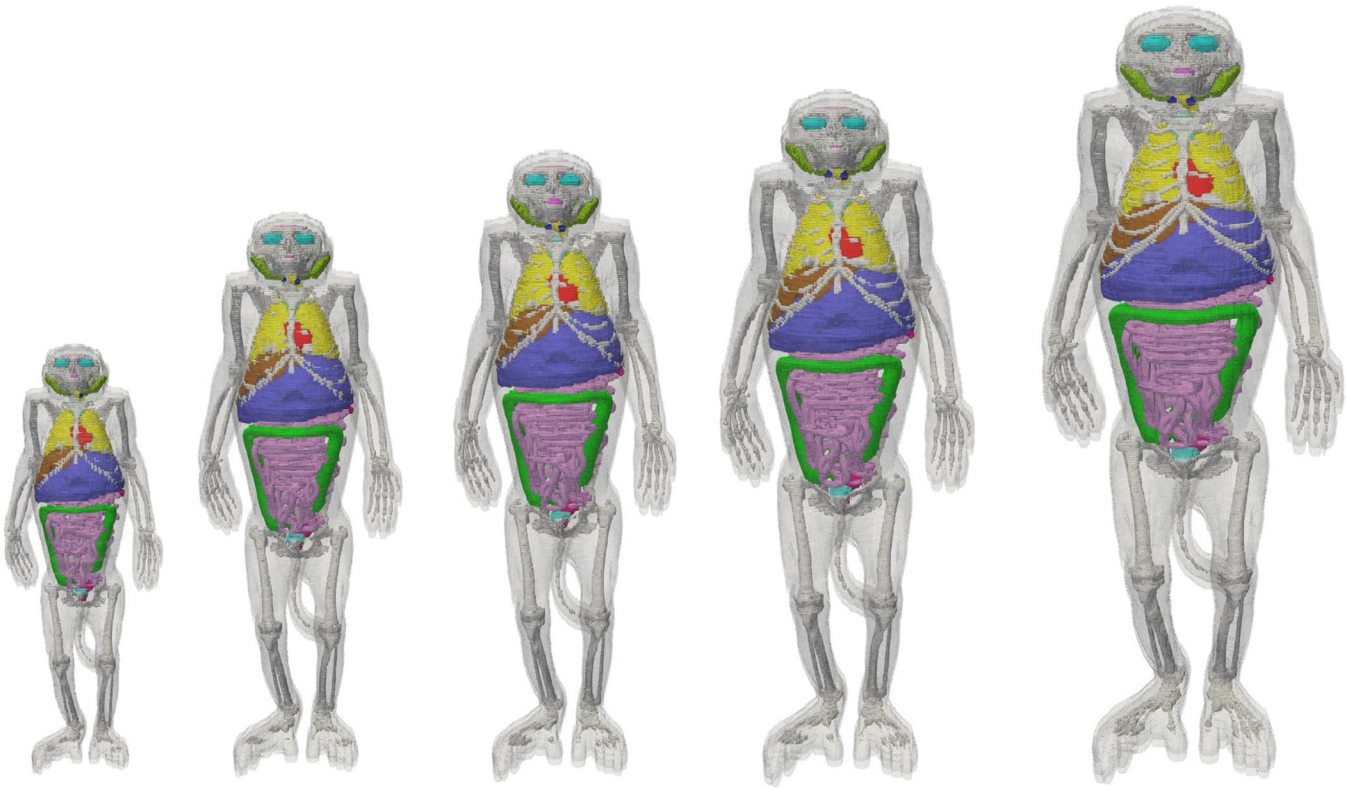

FIG. 1. Three-dimensional visualization of constructed NHP computational models at different ages. [Color figure can be viewed at wileyonlinelibrary.com]

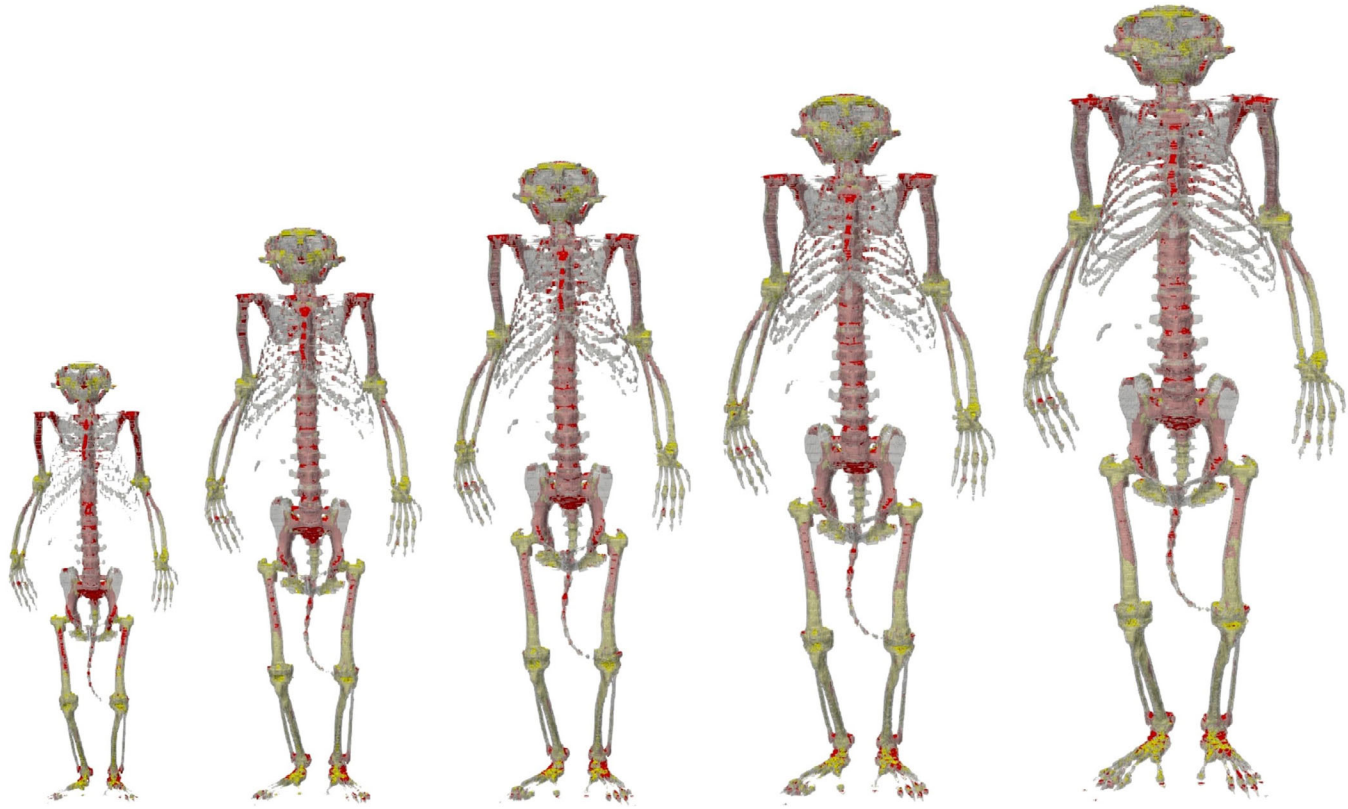

FIG. 2. Three-dimensional visualization of the skeleton system of the constructed NHP computational models at different ages. [Color figure can be viewed at wileyonlinelibrary.com]

and S-values of the investigated radionuclides are calculated for all source-target pairs.

A total of 1.0×10^7 primary particle histories were generated in each simulation where the statistical uncertainty of the results in most of the cases is <2% (the largest statistical uncertainties were at the cross-irradiation conditions for the eye lens/bladder content and range between 46% and 100%). The calculated S-values were used for calculation of the absorbed doses from radiotracers in the NHP subjects at different ages. The investigated radiotracers include ^{11}C-labeled brain receptor substances for molecular imaging of different brain receptors, realistic maximum of ^{11}C-labeled substances, ^{15}O-H_2O for blood flow measurement, ^{18}F-labeled brain receptor substances for molecular imaging of cerebral receptors, and ^{18}F-FDG (2-[^{18}F]Fluoro-2-deoxy-D-glucose) for glucose metabolism investigations. The biokinetic data of the considered radiotracers were obtained from ICRP reports.[22,23]

2.C. Dose calculations

The absorbed dose is the basic physical quantity used in radiation metrology, radiological protection, radiation biology, and clinical radiology. It is defined as the mean particle energy deposited in the target tissue per unit mass. In the Medical Internal Radiation Dose (MIRD) formalism,[24] the radiation absorbed dose delivered to target tissue from source organ can be estimated as:

$$D_T = \sum_i A_i S_{i\to T} \tag{2}$$

where D_T is the mean absorbed dose, A_i is the cumulative activity in the source organ i, $S_{i\to T}$ is the S-value reflecting the equivalent dose rate in the target organ per unit activity in the source organ. The calculation of S-values depends on the decay scheme of the considered radionuclide, the type, energy, and yield of emitted radiation per nuclear transformation, which can be defined as:

$$S_{i\to T} = \frac{1}{M_T} \sum_j E_j Y_j \Phi^j_{i\to T} \tag{3}$$

where M_T is the mass of the target organ and $\Phi^j_{i\to T}$ is the absorbed fraction of emission j in the target organ. E_j and Y_j are the individual energy and yield of each emitted radiation per nuclear transformation, respectively. The absorbed dose can be linked to biological effects and radiation risks for assessing the biological detriments from stochastic effects to different organs.

3. RESULTS

3.A. Developed NHP model series

Table II summarizes the calculated masses of the different organs of the constructed anatomic NHP models. The skin was generated by assigning a skin tag to the outermost voxel layer of the NHP body contour. The percent differences between body weight of the developed series of NHP models and the aimed reference values range between −0.02% and 0.05%. Figure 3 compares the average organ mass percentage of total body mass for the adrenals, brain, kidney, liver, lung, pancreas, spleen, and thyroid of the constructed NHP models in this work and an experimental estimation of the same organs reported by Stahl et al.[25] The mean mass percentage of the brain for the NHP model is 1.47%, while the corresponding experimental estimate ranges between 0.94% and 2.95%. The mean mass percentage of the liver is 2.23%, while the experimental estimate ranges between 1.91% and 4.10%. The mean mass percentage of the lung is 1.20% for the constructed NHP models while the corresponding estimate by Stahl et al.[25] ranges between 0.43% and 1.4%. The masses of mineral bone for the baby, infant, juvenile, young and adult NHP models are 73.92g, 171.79 g, 230.04 g, 350.36 g, and 574.96 g, respectively, with an average mass percentage of 7.2%. The masses of the RBM for the baby, infant, juvenile, young and adult NHP models are 32.18 g, 73.85 g, 102.69 g, 155.02 g, and 252.53 g, respectively, with an average mass percentage of 3.16%.

TABLE II. Organ masses of computational rhesus monkeys models.

	Masses (g)				
Organs	Baby	Infants	Juveniles	Young	Adult
Adrenals	0.11	0.30	0.40	0.70	0.99
Bladder wall	0.63	1.36	1.92	2.94	4.76
Brain	16.30	37.24	51.86	76.57	126.01
Breasts	0.17	0.45	0.51	0.93	1.50
Mineral bone	73.92	171.79	230.04	350.36	574.96
RBM	32.18	73.85	102.69	155.02	252.53
YBM	16.22	37.06	49.23	74.23	123.01
Esophagus	1.23	2.95	4.05	5.92	9.99
Eye balls	1.10	2.81	3.60	5.42	10.46
Eye lens	0.03	0.10	0.13	0.27	0.30
Gall bladder wall	0.06	0.14	0.20	0.31	0.48
Heart wall	8.73	20.44	28.21	42.01	69.40
Kidney	3.69	8.55	11.54	17.49	28.77
LI wall	8.94	21.52	28.95	44.08	73.97
Liver	24.48	56.49	77.99	116.24	191.52
Lung	13.30	30.74	41.80	62.92	102.53
Muscle	632.76	1462.24	1999.33	2988.85	4905.83
Ovaries	0.11	0.23	0.37	0.47	0.85
Pancreas	1.29	2.91	4.20	5.97	9.99
Salivary gland	4.25	9.44	13.41	20.62	31.72
SI wall	23.57	52.86	75.27	112.01	182.49
Skin	133.89	309.07	423.83	628.72	1040.01
Spinal cord	2.58	6.27	8.23	12.71	21.03
Spleen	0.54	1.20	1.74	2.48	4.16
Stomach wall	21.98	51.36	69.85	105.05	172.83
Thymus	0.41	0.82	1.10	1.63	2.78
Thyroid	0.12	0.27	0.40	0.59	0.86
Tongue	2.15	5.11	7.27	10.29	16.91
Uterus	1.09	2.50	3.24	4.99	8.72

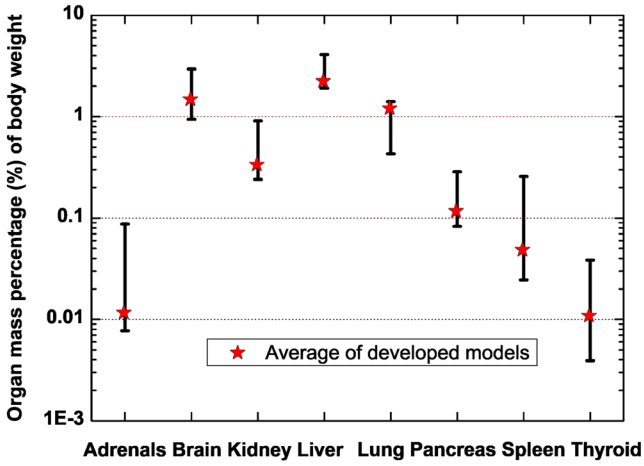

FIG. 3. Comparison between average organ mass percentage of body weight for the constructed NHP models in this work and those reported in experimental studies.[25] The upper and lower horizontal short lines represents the maximum and minimum values. [Color figure can be viewed at wileyonline library.com]

3.B. S-values for positron-emitting radionuclides

The S-values for C-11, N-13, O-15, F-18, Cu-64, Ga-68, Rb-82, Y-86, and I-124 were calculated for five computational NHP models where 33 identified organs/regions were adopted as both target and source organs. Figure 4 shows a plot of the self-absorbed S-values for C-11 and F-18 in the brain, kidney, colon, liver, lung, spleen, stomach, thyroid, ovaries, and uterus of the age-dependent NHP models with different body weights. As can be seen, the self-absorbed S-values decrease while the model weight increases. For the baby NHP model, the self-absorbed S-values of the brain from C-11 and F-18 are 6.8 and 7.0 times higher than the self-absorbed S-values of the brain in the adult NHP model, respectively. The highest observed self-absorbed S-values were in the ovaries of the baby NHP model (3.44E-01 mGy/MBq.s for F-18 and 4.79E-01 mGy/MBq.s for C-11, respectively), while the lowest self-absorbed S-values were in the liver of the adult NHP (2.59E-04 mGy/MBq.s for F-18 and 3.74E-04 mGy/MBq.s for C-11, respectively). Figure 5 shows the self-absorbed S-values for the lung and salivary glands from the considered radionuclides. At all age periods, the NHP lung presents the highest self-absorbed S-values from Rb-82, ranging between 1.54E-03 mGy/MBq.s and 8.29E-03 mGy/MBq.s, while the lowest self-absorbed S-value for the lung was produced by Cu-64 (ranging from 1.97E-04 mGy/MBq.s to 1.45E-03 mGy/MBq.s). For the salivary glands, the self-absorbed S-values of O-15 and Ga-68 are close together and about 56% higher than C-11, and would be about 2.3 times higher than the S-value of F-18. The skeleton contributes significantly to whole-body radiation risks, since the bone in the skeleton is an important dose-limiting tissue, expressing high radiosensitivity. It is important to investigate skeletal dosimetry for studies of radiation biology and radiological protection. Figure 6 shows the self-absorbed S-values for mineral bone, RBM, and YBM from C-11, F-18, and Cu-64. For the same radionuclide, the YBM presents the highest self-absorbed S-value while mineral bone presents the lowest self-absorbed S-value. The self-absorbed S-values of RBM and YBM for C-11, F-18, and Cu-64 are about 2.3 and 4.4 times higher than mineral bone, respectively. Figure 7 shows the cross-absorbed (source and target different) S-values for Ga-68 in the liver and total body. For the total body irradiating other organs, the cross-absorbed S-value in the lung is about 1.7–2.9 times higher than the S-values of other organs. When the source is in the liver, adjacent organs, such as adrenals, stomach, lung, and heart, present higher cross-absorbed S-values than other organs, whereas the bladder receives the lowest S-value (ranging from 1.77E-05 mGy/MBq.s to 1.22E-04 mGy/MBq.s). Figure 8 shows the cross-absorbed S-values from the total body to the brain and from the kidney to the liver for the considered radionuclides. At all considered age periods, the highest

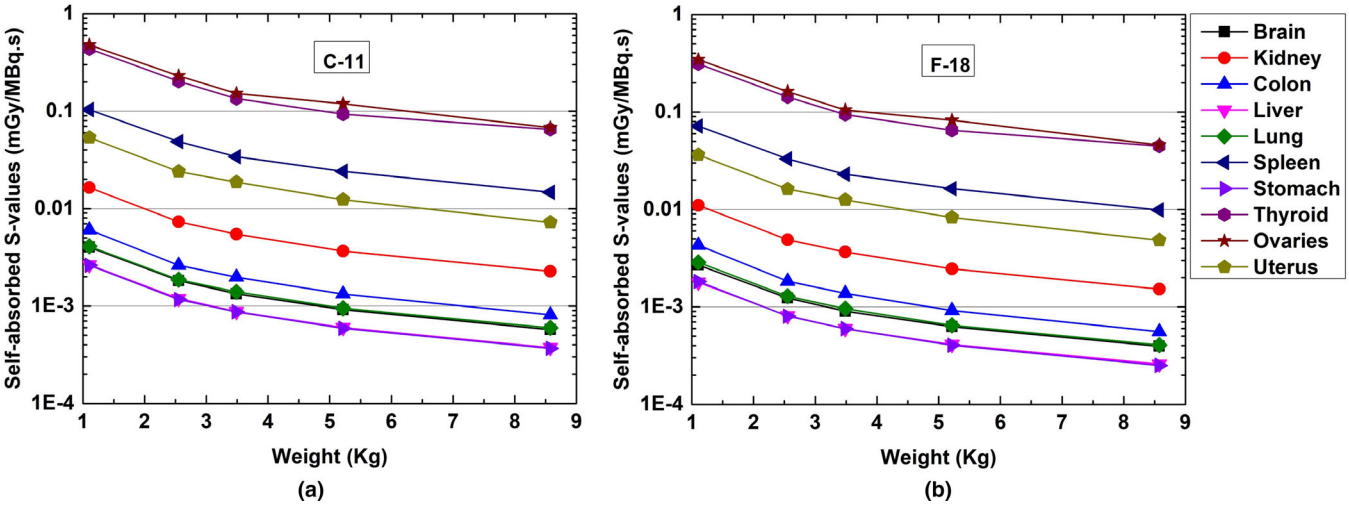

FIG. 4. Self-absorbed S-values for (a) C-11 and (b) F-18 for various organs. [Color figure can be viewed at wileyonlinelibrary.com]

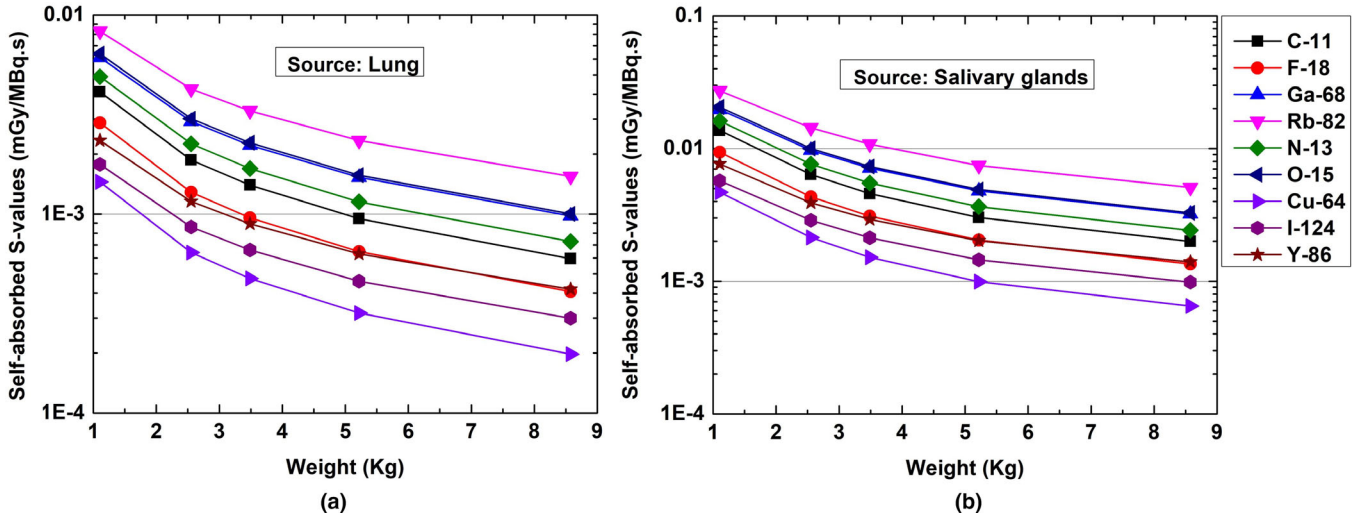

FIG. 5. Self-absorbed S-values for (a) the lung and (b) salivary glands for various radionuclides. [Color figure can be viewed at wileyonlinelibrary.com]

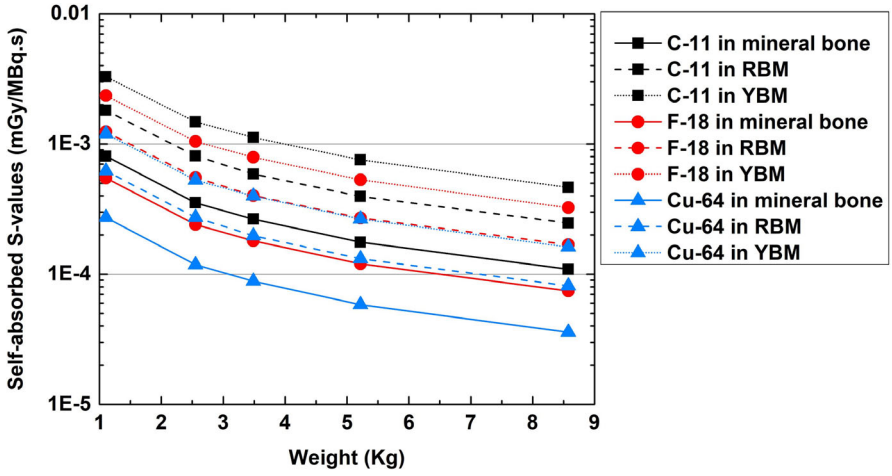

FIG. 6. Self-absorbed S-values for mineral bone, RBM, and YBM from C-11, F-18, and Cu-64. [Color figure can be viewed at wileyonlinelibrary.com]

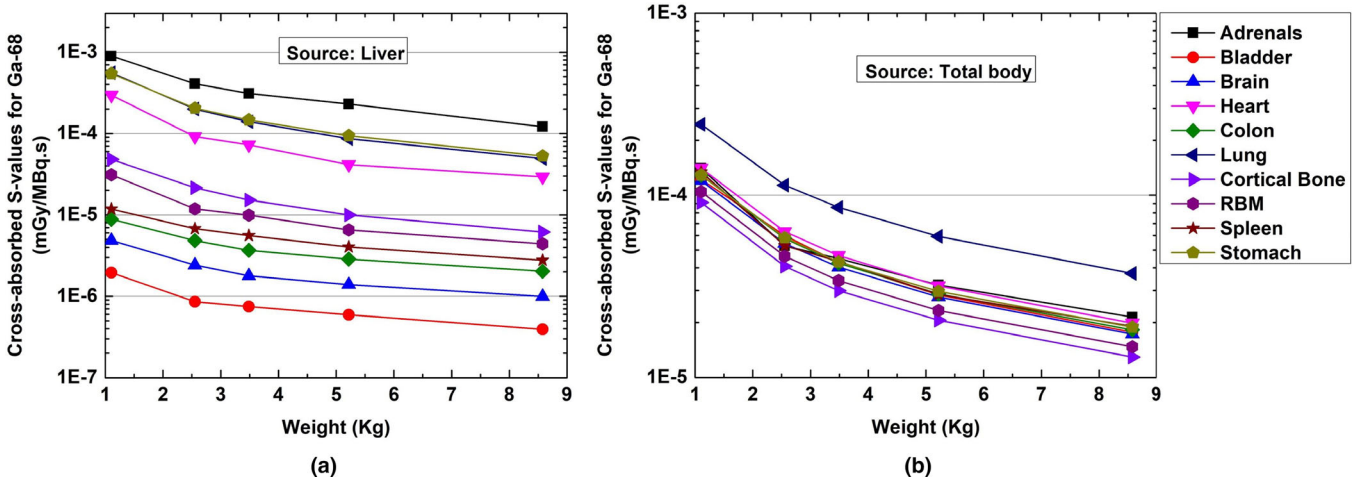

FIG. 7. Cross-absorbed S-values for Ga-68 to various organs from (a) the liver and (b) total body considered as source organs. [Color figure can be viewed at wileyonlinelibrary.com]

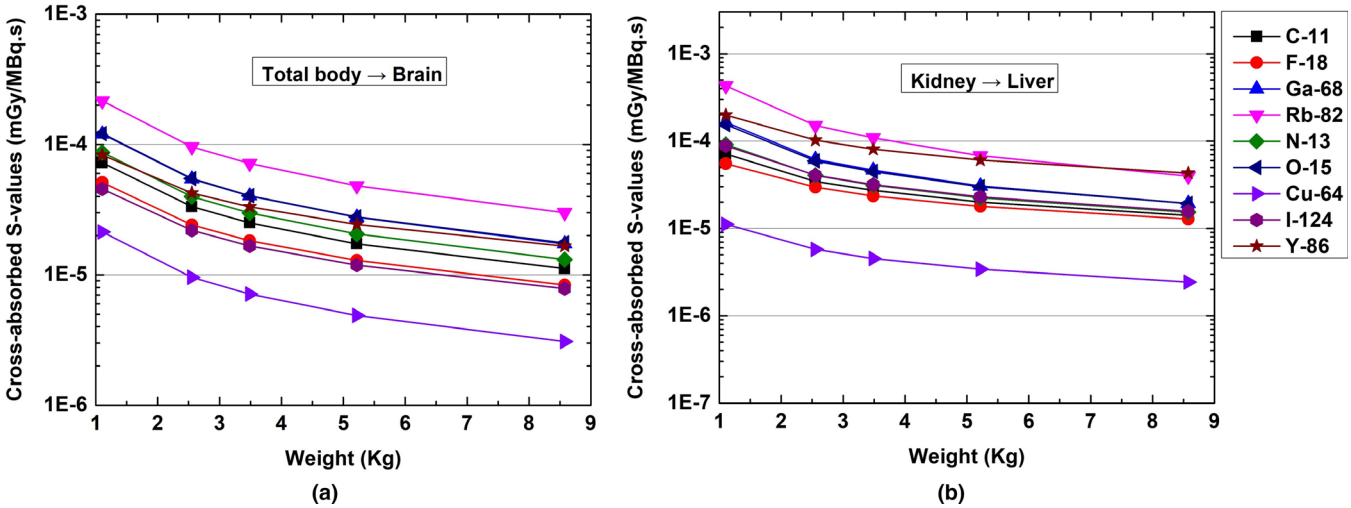

FIG. 8. Cross-absorbed S-values (a) from total body to brain and (b) from the kidney to liver for various radionuclides. [Color figure can be viewed at wileyonlinelibrary.com]

TABLE III. Absorbed dose for NHP models from ^{11}C-labeled brain receptor substances.

Absorbed dose (mGy/MBq)					
	^{11}C-labeled brain receptor substances				
Organs	Baby	Infants	Juveniles	Youngs	Adult
Muscle	1.13E-01	5.27E-02	3.95E-02	2.75E-02	1.77E-02
Skin	9.63E-02	4.40E-02	3.30E-02	2.29E-02	1.45E-02
Adrenals	1.19E-01	5.72E-02	4.17E-02	3.09E-02	1.91E-02
Bladder wall	1.58E+00	6.81E-01	5.99E-01	3.95E-01	2.22E-01
Brain	3.22E-01	1.47E-01	1.08E-01	7.48E-02	4.73E-02
Breasts	1.13E-01	5.23E-02	3.68E-02	2.78E-02	1.76E-02
Esophagus	1.25E-01	5.78E-02	4.40E-02	3.12E-02	2.02E-02
Eye balls	1.13E-01	5.17E-02	3.90E-02	2.71E-02	1.77E-02
Eye lens	1.15E-01	5.17E-02	3.76E-02	2.67E-02	1.74E-02
Gall bladder wall	1.21E-01	5.52E-02	4.34E-02	3.06E-02	2.03E-02
Heart wall	1.26E-01	5.83E-02	4.39E-02	3.07E-02	1.99E-02
Kidney	1.20E-01	5.63E-02	4.21E-02	2.99E-02	1.90E-02
LI wall	1.19E-01	5.66E-02	4.23E-02	2.96E-02	1.93E-02
Liver	1.21E-01	5.60E-02	4.22E-02	2.96E-02	1.92E-02
Lung	2.33E-01	1.08E-01	8.06E-02	5.59E-02	3.55E-02
Pancreas	1.22E-01	5.76E-02	4.37E-02	3.09E-02	1.97E-02
Salivary gland	1.17E-01	5.50E-02	4.16E-02	2.87E-02	1.86E-02
SI wall	1.28E-01	6.14E-02	4.49E-02	3.15E-02	2.06E-02
Mineral bone	8.00E-02	3.77E-02	2.85E-02	2.00E-02	1.32E-02
RBM	9.80E-02	4.56E-02	3.45E-02	2.41E-02	1.57E-02
YBM	1.08E-01	4.96E-02	3.73E-02	2.58E-02	1.66E-02
Spinal cord	1.17E-01	5.49E-02	4.15E-02	2.91E-02	1.91E-02
Spleen	1.15E-01	5.48E-02	4.04E-02	2.89E-02	1.83E-02
Stomach wall	1.18E-01	5.48E-02	4.13E-02	2.87E-02	1.86E-02
Thymus	1.19E-01	5.85E-02	4.19E-02	2.97E-02	1.97E-02
Thyroid	1.21E-01	5.42E-02	4.03E-02	3.03E-02	1.91E-02
Tongue	1.10E-01	5.06E-02	3.88E-02	2.70E-02	1.75E-02
Ovaries	1.27E-01	6.01E-02	4.59E-02	3.16E-02	2.16E-02
Uterus	1.56E-01	7.65E-02	5.93E-02	4.12E-02	2.72E-02
GI tract	1.23E-01	5.79E-02	4.30E-02	3.01E-02	1.96E-02
Total body	1.23E-01	5.71E-02	4.28E-02	2.98E-02	1.91E-02

TABLE IV. Absorbed dose for NHP models from ^{11}C-labeled substances (realistic maximum).

Absorbed dose (mGy/MBq)					
	^{11}C-labeled substances (realistic maximum)				
Organs	Baby	Infants	Juveniles	Youngs	Adult
Muscle	8.56E-02	4.10E-02	3.08E-02	2.19E-02	1.45E-02
Skin	6.38E-02	2.96E-02	2.24E-02	1.57E-02	1.01E-02
Adrenals	7.31E-02	3.53E-02	2.61E-02	1.90E-02	1.18E-02
Bladder wall	8.24E+00	3.54E+00	3.14E+00	2.06E+00	1.15E+00
Brain	6.54E-02	3.01E-02	2.27E-02	1.56E-02	1.01E-02
Breasts	6.83E-02	3.17E-02	2.22E-02	1.68E-02	1.06E-02
Esophagus	7.57E-02	3.48E-02	2.64E-02	1.87E-02	1.21E-02
Eye balls	6.52E-02	2.95E-02	2.22E-02	1.53E-02	9.97E-03
Eye lens	6.71E-02	2.99E-02	2.16E-02	1.53E-02	9.97E-03
Gall bladder wall	7.40E-02	3.38E-02	2.65E-02	1.87E-02	1.23E-02
Heart wall	7.58E-02	3.52E-02	2.64E-02	1.85E-02	1.20E-02
Kidney	7.51E-02	3.52E-02	2.63E-02	1.87E-02	1.20E-02
LI wall	1.08E-01	5.40E-02	4.14E-02	2.95E-02	2.00E-02
Liver	7.37E-02	3.43E-02	2.57E-02	1.81E-02	1.17E-02
Lung	1.41E-01	6.49E-02	4.84E-02	3.36E-02	2.14E-02
Pancreas	7.58E-02	3.60E-02	2.72E-02	1.93E-02	1.24E-02
Salivary gland	6.83E-02	3.18E-02	2.39E-02	1.64E-02	1.06E-02
SI wall	9.14E-02	4.48E-02	3.31E-02	2.42E-02	1.63E-02
Mineral bone	6.05E-02	2.93E-02	2.25E-02	1.60E-02	1.08E-02
RBM	7.05E-02	3.36E-02	2.59E-02	1.85E-02	1.22E-02
YBM	7.54E-02	3.55E-02	2.71E-02	1.90E-02	1.25E-02
Spinal cord	7.18E-02	3.37E-02	2.54E-02	1.78E-02	1.18E-02
Spleen	7.16E-02	3.40E-02	2.50E-02	1.79E-02	1.14E-02
Stomach wall	7.25E-02	3.37E-02	2.53E-02	1.77E-02	1.14E-02
Thymus	7.13E-02	3.49E-02	2.49E-02	1.76E-02	1.17E-02
Thyroid	7.13E-02	3.17E-02	2.36E-02	1.76E-02	1.11E-02
Tongue	6.54E-02	2.98E-02	2.28E-02	1.58E-02	1.02E-02
Ovaries	1.46E-01	7.30E-02	5.65E-02	4.12E-02	2.84E-02
Uterus	2.94E-01	1.61E-01	1.34E-01	9.43E-02	6.32E-02
GI tract	8.62E-02	4.17E-02	3.13E-02	2.24E-02	1.49E-02
Total body	1.31E-01	6.07E-02	4.56E-02	3.18E-02	2.04E-02

cross-absorbed S-values for the total body irradiating the brain were produced by Rb-82 (varying between 3.00E-05 mGy/MBq.s and 2.16E-04 mGy/MBq.s), while the lowest cross-absorbed S-values of the brain were produced by Cu-64 (ranging between 3.08E-06 mGy/MBq.s and 2.13E-05 mGy/MBq.s). The relative differences in S-values per kg difference in body weight (%/kg) for C-11 and F-18 between the baby NHP model and adult NHP model are summarized in supplemental Tables S1 and S2, respectively. For most source-target organ pairs, the relative difference of C-11 S-values ranges between −13.4% and −8.8%/kg difference in body weight while the relative difference of F-18 S-values was between −12.9% and −8.0%/kg difference in body weight. The mean relative difference is about −10.6%/kg for considered source-target pairs.

TABLE V. Absorbed dose for NHP models from ^{15}O-H_2O.

Absorbed dose (mGy/MBq)					
	^{15}O-H_2O				
Organs	Baby	Infants	Juveniles	Youngs	Adult
Muscle	1.63E-02	7.34E-03	5.46E-03	3.75E-03	2.36E-03
Skin	1.19E-02	5.52E-03	4.11E-03	2.86E-03	1.82E-03
Adrenals	9.51E-02	4.28E-02	3.47E-02	2.16E-02	1.55E-02
Bladder wall	1.58E-02	6.59E-03	5.41E-03	3.46E-03	2.18E-03
Brain	9.17E-02	4.18E-02	3.05E-02	2.10E-02	1.31E-02
Breasts	1.48E-02	7.76E-03	6.00E-03	3.51E-03	2.39E-03
Esophagus	2.27E-02	9.34E-03	6.95E-03	4.81E-03	3.07E-03
Eye balls	1.58E-02	7.05E-03	5.42E-03	3.66E-03	2.38E-03
Eye lens	1.42E-02	7.13E-03	5.13E-03	3.45E-03	2.19E-03
Gall bladder wall	4.93E-02	1.99E-02	1.40E-02	9.41E-03	5.57E-03
Heart wall	4.08E-02	1.78E-02	1.32E-02	8.96E-03	5.61E-03
Kidney	1.05E-01	4.80E-02	3.59E-02	2.44E-02	1.53E-02
LI wall	3.82E-02	1.76E-02	1.35E-02	9.27E-03	5.83E-03
Liver	9.07E-02	4.10E-02	3.03E-02	2.07E-02	1.29E-02
Lung	8.11E-02	3.76E-02	2.84E-02	1.94E-02	1.24E-02
Pancreas	6.92E-02	3.30E-02	2.40E-02	1.70E-02	1.08E-02
Salivary gland	1.66E-02	7.40E-03	5.72E-03	3.92E-03	2.53E-03
SI wall	2.78E-02	1.28E-02	9.34E-03	6.51E-03	4.15E-03
Mineral bone	1.92E-02	8.53E-03	6.41E-03	4.33E-03	2.75E-03
RBM	1.56E-02	6.91E-03	5.18E-03	3.51E-03	2.24E-03
YBM	1.63E-02	7.33E-03	5.36E-03	3.66E-03	2.30E-03
Spinal cord	1.73E-02	8.00E-03	6.01E-03	4.14E-03	2.70E-03
Spleen	3.08E-01	1.54E-01	1.10E-01	7.91E-02	4.92E-02
Stomach wall	1.77E-02	7.60E-03	5.65E-03	3.87E-03	2.42E-03
Thymus	1.98E-02	9.64E-03	6.43E-03	4.42E-03	2.82E-03
Thyroid	1.24E-01	6.26E-02	4.33E-02	3.08E-02	2.24E-02
Tongue	1.56E-02	6.97E-03	5.40E-03	3.58E-03	2.30E-03
Ovaries	3.91E-02	1.94E-02	1.43E-02	1.03E-02	6.54E-03
Uterus	1.71E-02	7.49E-03	5.38E-03	3.53E-03	2.33E-03
GI tract	2.54E-02	1.14E-02	8.51E-03	5.89E-03	3.72E-03
Total body	2.08E-02	9.41E-03	7.01E-03	4.81E-03	3.04E-03

3.C. Absorbed doses from radiotracers

Absorbed doses of 33 organs from the considered positron-emitting radiotracers were evaluated for the constructed NHP computational models. Tables III–VII summarize the calculated organ absorbed doses for ^{11}C-labeled brain receptor substances, ^{11}C-labeled substances (realistic maximum), ^{15}O-H_2O, ^{18}F-labeled brain receptor substances, and ^{18}F-FDG, respectively. The highest absorbed dose to critical organs was observed in the bladder for ^{11}C-labeled brain receptor substances, ^{11}C-labeled substances (realistic maximum model) and ^{18}F-FDG; the spleen and kidney for ^{15}O-H_2O; and the thyroid and kidney for ^{18}F-labeled brain receptor substances, respectively. For most targeted regions, ^{15}O-H_2O produces the lowest absorbed dose because of its short half-life (2 min). For the adult NHP's brain, the absorbed dose of ^{18}F-labeled brain receptor substances is 5.2 times higher than ^{11}C-labeled brain receptor substances, and 18.8 times higher than the

TABLE VI. Absorbed dose for NHP models from ^{18}F-labeled brain receptor substances.

Absorbed dose (mGy/MBq)					
	^{18}F-labeled brain receptor substances				
Organs	Baby	Infants	Juveniles	Youngs	Adult
Muscle	4.08E-01	1.93E-01	1.47E-01	1.04E-01	6.79E-02
Skin	3.44E-01	1.60E-01	1.21E-01	8.44E-02	5.44E-02
Adrenals	5.05E-01	2.46E-01	1.91E-01	1.37E-01	9.30E-02
Bladder wall	2.63E+00	1.30E+00	1.16E+00	8.24E-01	5.15E-01
Brain	1.64E+00	7.55E-01	5.56E-01	3.89E-01	2.47E-01
Breasts	4.23E-01	1.95E-01	1.51E-01	1.08E-01	6.76E-02
Esophagus	4.91E-01	2.37E-01	1.83E-01	1.31E-01	8.72E-02
Eye balls	4.18E-01	1.99E-01	1.52E-01	1.08E-01	7.14E-02
Eye lens	3.98E-01	1.95E-01	1.44E-01	9.89E-02	6.87E-02
Gall bladder wall	5.87E-01	2.86E-01	2.18E-01	1.57E-01	1.09E-01
Heart wall	4.83E-01	2.32E-01	1.79E-01	1.27E-01	8.48E-02
Kidney	2.38E+00	1.07E+00	8.06E-01	5.47E-01	3.45E-01
LI wall	4.35E-01	2.08E-01	1.58E-01	1.12E-01	7.40E-02
Liver	1.29E+00	5.95E-01	4.43E-01	3.08E-01	1.97E-01
Lung	1.29E+00	5.93E-01	4.47E-01	3.07E-01	1.97E-01
Pancreas	4.81E-01	2.37E-01	1.82E-01	1.29E-01	8.69E-02
Salivary gland	4.40E-01	2.12E-01	1.63E-01	1.17E-01	7.63E-02
SI wall	2.83E-01	1.44E-01	1.09E-01	7.95E-02	5.45E-02
Mineral bone	2.93E-01	1.44E-01	1.10E-01	7.99E-02	5.37E-02
RBM	3.64E-01	1.76E-01	1.35E-01	9.64E-02	6.43E-02
YBM	3.93E-01	1.86E-01	1.40E-01	9.87E-02	6.40E-02
Spinal cord	4.48E-01	2.17E-01	1.66E-01	1.20E-01	7.91E-02
Spleen	4.09E-01	1.97E-01	1.53E-01	1.07E-01	6.81E-02
Stomach wall	4.41E-01	2.08E-01	1.59E-01	1.12E-01	7.36E-02
Thymus	4.68E-01	2.26E-01	1.72E-01	1.21E-01	8.08E-02
Thyroid	5.25E+00	2.42E+00	1.61E+00	1.11E+00	7.71E-01
Tongue	4.01E-01	1.92E-01	1.45E-01	1.03E-01	6.77E-02
Ovaries	4.64E-01	2.16E-01	1.72E-01	1.22E-01	8.23E-02
Uterus	5.76E-01	2.89E-01	2.33E-01	1.61E-01	1.09E-01
GI tract	3.74E-01	1.83E-01	1.38E-01	9.87E-02	6.60E-02
Total body	4.59E-01	2.16E-01	1.64E-01	1.15E-01	7.53E-02

absorbed dose from ^{15}O-H_2O. For ^{18}F-FDG, the absorbed dose to the kidney, liver, and brain of the baby NHP model are 5.8, 6.4, and 6.7 times higher than the corresponding absorbed doses to the adult model. The calculated absorbed doses from ^{18}F-labeled brain receptor substances to the NHP brain are 1.64, 0.76, 0.56, 0.39, and 0.25 mGy/MBq in the baby model, infants model, juvenile model, young model, and adult model, respectively, while the ^{11}C- labeled brain receptor substances to the NHP brain are 0.32, 0.15, 0.11, 0.075, and 0.047 mGy/MBq in the corresponding models, respectively. For mineral bone and RBM, the absorbed doses of ^{18}F-FDG in the NHP models range from 0.051 to 0.27 mGy/MBq and from 0.061 to 0.34 mGy/MBq, respectively.

4. DISCUSSION

Accurate radiation dose calculations for NHP subjects in preclinical research are required for dose regimen optimization of radiotracers and investigation of collective radiation risks associated with diagnostic radiology and nuclear medicine procedures. However, when living and growing subjects are used in radiological protection, radiation biology, and clinical diagnostic imaging studies, discrepancies might occur between the actual anatomy of laboratory animals and the employed computational models. Similar to other laboratory animals, NHPs may present different bioavailability and radiosensitivity to ionizing radiation at different age periods.[14] The evaluation of age-dependent radiation dosimetry to laboratory specimens is required. In this work, we developed NHP model series based on NURBS geometries to represent NHP subjects at different ages. Morphological parameters, including body weight and crown-rump length of the constructed models fit well with the corresponding reference values reported in literature.[15] The organ masses of the developed models were within the range reported in experimental studies.[25] Based on the developed

TABLE VII. Absorbed dose for NHP models from ^{18}F-FDG.

Absorbed dose (mGy/MBq)					
	^{18}F-FDG				
Organs	Baby	Infants	Juveniles	Youngs	Adult
Muscle	3.77E-01	1.80E-01	1.37E-01	9.70E-02	6.37E-02
Skin	3.15E-01	1.48E-01	1.11E-01	7.81E-02	5.06E-02
Adrenals	4.23E-01	2.06E-01	1.59E-01	1.13E-01	7.65E-02
Bladder wall	3.26E+00	1.61E+00	1.45E+00	1.03E+00	6.44E-01
Brain	2.12E+00	9.74E-01	7.16E-01	5.00E-01	3.16E-01
Breasts	4.02E-01	1.88E-01	1.45E-01	1.04E-01	6.60E-02
Esophagus	4.74E-01	2.32E-01	1.80E-01	1.30E-01	8.69E-02
Eye balls	3.97E-01	1.91E-01	1.46E-01	1.04E-01	6.90E-02
Eye lens	3.76E-01	1.84E-01	1.36E-01	9.37E-02	6.54E-02
Gall bladder wall	5.20E-01	2.53E-01	1.95E-01	1.40E-01	9.78E-02
Heart wall	2.10E+00	9.48E-01	7.04E-01	4.88E-01	3.10E-01
Kidney	4.07E-01	1.96E-01	1.50E-01	1.06E-01	7.05E-02
LI wall	4.07E-01	1.97E-01	1.49E-01	1.06E-01	7.08E-02
Liver	9.78E-01	4.54E-01	3.40E-01	2.38E-01	1.54E-01
Lung	1.00E+00	4.66E-01	3.52E-01	2.45E-01	1.58E-01
Pancreas	4.16E-01	2.01E-01	1.55E-01	1.10E-01	7.41E-02
Salivary gland	4.13E-01	2.00E-01	1.54E-01	1.11E-01	7.28E-02
SI wall	4.02E-01	1.94E-01	1.47E-01	1.05E-01	7.03E-02
Mineral bone	2.77E-01	1.37E-01	1.05E-01	7.64E-02	5.15E-02
RBM	3.40E-01	1.65E-01	1.27E-01	9.07E-02	6.06E-02
YBM	3.63E-01	1.73E-01	1.30E-01	9.22E-02	6.00E-02
Spinal cord	4.13E-01	2.01E-01	1.54E-01	1.12E-01	7.35E-02
Spleen	3.76E-01	1.82E-01	1.41E-01	9.87E-02	6.33E-02
Stomach wall	4.06E-01	1.96E-01	1.50E-01	1.07E-01	7.07E-02
Thymus	4.50E-01	2.20E-01	1.69E-01	1.20E-01	8.03E-02
Thyroid	4.21E-01	2.09E-01	1.56E-01	1.12E-01	7.56E-02
Tongue	3.72E-01	1.79E-01	1.36E-01	9.61E-02	6.36E-02
Ovaries	4.40E-01	2.09E-01	1.66E-01	1.18E-01	7.97E-02
Uterus	5.86E-01	3.00E-01	2.44E-01	1.69E-01	1.14E-01
GI tract	4.06E-01	1.96E-01	1.49E-01	1.07E-01	7.09E-02
Total body	4.61E-01	2.18E-01	1.65E-01	1.16E-01	7.59E-02

computational NHP models, we estimated S-values for nine positron-emitting radionuclides. Both self-absorbed and cross-absorbed S-values for identified organs decrease with the NHP body weight. The absorbed doses from five positron-emitting labeled radiotracers were estimated based on the standard MIRD formalism. Similar administered activities result in significantly higher absorbed dose in the young NHP than in the adult NHP as a consequence of the organs being smaller and in closer proximity to each other. Given that young animals are commonly more radiosensitive, this in turn results in higher radiation risks for young specimens. In this regard, understanding the correlation between the absorbed dose and changes in body weight and age is important for determining the therapeutic effects and radiotoxicities of radiotracers in experimental research. Among all considered radiotracers, the difference between organ absorbed doses from the baby NHP model to the adult NHP model ranges between −11.9% and −10.5% per kg difference in body weight, with an average difference of −11.2% per kg. The organ absorbed dose in low-weight young animals is considerably higher than that in the adult animal.

In vivo molecular imaging using NHPs was promoted as an exciting line of research for the design of longitudinal studies and the development of novel imaging techniques. Considering the link to translational studies, NHPs can be phylogenetically correlated with human beings and have been considered as the closest relatives of humans in biomedical research. However, the radiation dose to NHPs in preclinical research was rarely studied. The radiation dosimetry data produced in this work enable researchers to estimate the absorbed doses to NHPs from experimental molecular imaging studies. For instance, the study by Chefer et al.[26] used ^{18}F-FDG PET/CT imaging using NHPs for monitoring infection development of MERS-CoV, where four rhesus macaques were injected with 9-10 MBq/kg of ^{18}F-FDG in nine imaging sessions on preinoculation days and postinoculation

days. The cumulated absorbed dose to the bladder, brain, heart, lung, and kidney of the studied rhesus macaques can be calculated according to data provided in Table VII, namely 410–455 mGy, 202–225 mGy, 199–221 mGy, 100–111 mGy, and 42–47 mGy, respectively. Considering that absorbed doses of more than 50 mGy may affect the innate immune response in mammal subjects,[11] the absorbed dose to laboratory animals in preclinical research should not be overlooked, especially when the study design involves serial or repeated molecular imaging procedures.

5. CONCLUSIONS

We evaluated the variability of the radiation dose delivered to NHPs from positron-emitting radionuclides and radiotracers with age-related body weight. The S-values of commonly used positron-emitting radionuclides and the absorbed doses of five radiotracers present an inverse correlation with body weight. For most organs, the considered radionuclides and radiotracers produce significantly higher absorbed dose in low-weight young animals than in adult animals. Animal radiation dosimetry should be evaluated more thoroughly in longitudinal and translational studies involving repeated molecular imaging procedures as NHP specimens may receive non-negligible radiation doses, especially when young laboratory animals are used. The generated S-values of positron-emitting radionuclides and absorbed doses from radiotracers can be further exploited for radiation dosimetry of NHP specimens in preclinical research.

ACKNOWLEDGMENTS

This study was supported by the start-up grant from Fudan University to T. X., Swiss National Science Foundation under grant SNFN 320030_176052, Qatar national research fund (NPRP10-0126-170263), and the National Key R&D Program of China (Grant no. 2016YFF0200804).

CONFLICT OF INTEREST

The authors declare that they have no conflict of interest.

COMPLIANCE WITH ETHICAL STANDARDS

All applicable international, national, and/or institutional guidelines for the care and use of animals were followed. The study protocol was reviewed and approved by the Institutional Review Board (IRB) of National Primate Research Center of Korea Research Institute of Bioscience and Biotechnology (IRB No. KRIBB-AEC-18087). Written informed consent was not required for this study.

[a]Author to whom correspondence should be addressed. Electronic mail: tianwuxie@fudan.edu.cn; Telephone: +86 21 6404 8363; Fax: +86 21 6404 8363.

REFERENCES

1. Weerts EM, Fantegrossi WE, Goodwin AK. The value of nonhuman primates in drug abuse research. *Exp Clin Psychopharmacol*. 2007;15:309.
2. Berger B, Gaspar P, Verney C. Dopaminergic innervation of the cerebral cortex: unexpected differences between rodents and primates. *Trends Neurosci*. 1991;14:21–27.
3. Lile JA, Wang Z, Woolverton WL, et al. The reinforcing efficacy of psychostimulants in rhesus monkeys: the role of pharmacokinetics and pharmacodynamics. *J Pharmacol Exp Ther*. 2003;307:356–366.
4. Nader MA, Czoty PW. PET imaging of dopamine D2 receptors in monkey models of cocaine abuse: genetic predisposition versus environmental modulation. *Am J Psychiatry*. 2005;162:1473–1482.
5. Gould RW, Porrino LJ, Nader MA. Nonhuman primate models of addiction and PET imaging: dopamine system dysregulation. *Curr Top Behav Neurosci*. 2011;11:25–44.
6. Ma Y, Johnston TH, Peng S et al Reproducibility of a Parkinsonism-related metabolic brain network in non-human primates: a descriptive pilot study with FDG PET. *Mov Disord*. 2015;30:1283–1288.
7. Borghammer P, Chakravarty M, Jonsdottir KY et al Cortical hypometabolism and hypoperfusion in Parkinson's disease is extensive: probably even at early disease stages. *Brain Struct Funct*. 2010;214:303–317.
8. Murnane KS, Votaw JR, Howell LL. Acute brain metabolic effects of cocaine in rhesus monkeys with a history of cocaine use. *Brain Imaging Behav*. 2010;4:212–219.
9. Verschuer JD, Towson J, Eberl S et al Radiation dosimetry of the translocator protein ligands [18F] PBR111 and [18F] PBR102. *Nucl Med Biol*. 2012;39:742–753.
10. Bélanger MJ, Krause SM, Ryan C et al Biodistribution and radiation dosimetry of [18F]F-PEB in nonhuman primates. *Nucl Med Commun*. 2008;29:915–919.
11. Ha CT, Li X-H, Fu D et al Circulating interleukin-18 as a biomarker of total-body radiation exposure in mice, minipigs, and nonhuman primates (NHP). *PLoS One*. 2014;9:e109249.
12. Zaidi H, Xu XG. Computational anthropomorphic models of the human anatomy: the path to realistic Monte Carlo modeling in medical imaging. *Annu Rev Biomed Eng*. 2007;9:471–500.
13. Xie T, Park JS, Zhuo W, Zaidi H. Development of a nonhuman primate computational phantom for radiation dosimetry. *Med Phys*. 2020;47:736–744.
14. Xie T, Zaidi H. Age-dependent small-animal internal radiation dosimetry. *Mol Imaging*. 2013;12:364–375.
15. Andrade MCR, Ribeiro CT, Silva VFD et al Biologic data of *Macaca mulatta*, *Macaca fascicularis*, and Saimiri sciureusused for research at the fiocruz primate center. *Mem Inst Oswaldo Cruz*. 2004;99:584–589.
16. Valentin J. Basic anatomical and physiological data for use in radiological protection: reference values: ICRP Publication 89. *Ann ICRP*. 2002;32:1–277.
17. Min P. Binvox code-3D mesh voxelizer; 2011. https://www.patrickmin.com/binvox/ Accessed.
18. Nooruddin FS, Turk G. Simplification and repair of polygonal models using volumetric techniques. *IEEE Trans Vis Comput Graph*. 2003;9:191–205.
19. Xie T, Han D, Liu Y, Sun W, Liu Q. Skeletal dosimetry in a voxel-based rat phantom for internal exposures to photons and electrons. *Med Phys*. 2010;37:2167–2178.
20. Waters LS. MCNPX user's manual. Los Alamos National Laboratory, Report LA-CP-05-0369; 2005.
21. HPS. Radionuclide decay data. http://hps.org/publicinformation/radardecaydata.cfm
22. Valentin J. ICRP Publication 80: radiation dose to patients from radiopharmaceuticals. (Addendum 3 to ICRP Publication 53). *Ann ICRP*. 1998;28:1.
23. Valentin J. ICRP Publication 106: radiation dose to patients from radiopharmaceuticals. (Addendum 3 to ICRP Publication 53). *Ann ICRP*. 2008;38:126.
24. Bolch WE, Eckerman KF, Sgouros G, Thomas SR. MIRD pamphlet no. 21: a generalized schema for radiopharmaceutical dosimetry—standardization of nomenclature. *J Nucl Med*. 2009;50:477–484.
25. Stahl WR. Organ weights in primates and other mammals. *Science*. 1965;150:1039–1042.

26. Chefer S, Thomasson D, Seidel J et al Modeling [18 F]-FDG lymphoid tissue kinetics to characterize nonhuman primate immune response to Middle East respiratory syndrome-coronavirus aerosol challenge. *EJNMMI Res*. 2015;5:65.

SUPPORTING INFORMATION

Additional supporting information may be found online in the Supporting Information section at the end of the article.

Table S1. Percent difference between C-11 S Values per kg difference (%/kg) in total body mass from the baby to the adult NHP model.

Table S2. Percent difference between F-18 S Values per kg difference (%/kg) in total body mass from the baby to the adult NHP model.